JASA ARTICLE

Acoustofluidic device for acoustic capture of *Bacillus anthracis* spore analogues at low concentration[a)]

Filip Plazonic,[1] Adam Fisher,[1] Dario Carugo,[2] Martyn Hill,[1,b)] and Peter Glynne-Jones[1,c)]
[1]*Mechatronics, Faculty of Engineering and Physical Sciences, University of Southampton, Southampton, SO17 1BJ, United Kingdom*
[2]*Department of Pharmaceutics, UCL School of Pharmacy, University College London (UCL), London, WC1N 1AX, United Kingdom*

ABSTRACT:
A portable device for the rapid concentration of *Bacillus subtilis var niger* spores, also known as *Bacillus globigii* (BG), using a thin-reflector acoustofluidic configuration is described. BG spores form an important laboratory analog for the *Bacillus anthracis* spores, a serious health and bioterrorism risk. Existing systems for spore detection have limitations on detection time and detection that will benefit from the combination with this technology. Thin-reflector acoustofluidic devices can be cheaply and robustly manufactured and provide a more reliable acoustic force than previously explored quarter-wave resonator systems. The system uses the acoustic forces to drive spores carried in sample flows of 30 ml/h toward an antibody functionalized surface, which captures and immobilizes them. In this implementation, spores were fluorescently labeled and imaged. Detection at concentrations of 100 CFU/ml were demonstrated in an assay time of 10 min with 60% capture. We envisage future systems to incorporate more advanced detection of the concentrated spores, leading to rapid, sensitive detection in the presence of significant noise. © *2021 Acoustical Society of America*. https://doi.org/10.1121/10.0005278

(Received 31 March 2021; revised 21 May 2021; accepted 27 May 2021; published online 15 June 2021)
[Editor: Kedar Chitale] Pages: 4228–4238

I. INTRODUCTION

Inhalation anthrax is a form of anthrax poisoning that is mostly associated with bioterrorism.[1] Its cause is a bacteria called *Bacillus anthracis*. It is an oblong, nonmotile aerobic bacteria that is, on average, 1.42 μm long and 0.81 μm wide.[2] Inhalation anthrax is characterized by a delayed onset, followed by mild "flu-like" symptoms such as fever, fatigue, and a cough. This phase is abruptly replaced by much more severe symptoms, which include high fever, cyanosis, shock, extreme shortness of breath, and pleural effusion. In fatal cases, the pulse becomes extremely rapid and faint, the patient becomes highly disoriented, which is quickly followed by coma and death, occurring within 48 h from the onset of the second stage.[3] The mortality rate for this type of anthrax exposure used to be very high with >95%, but in recent years, with good access to antibiotics and medical care, the rate has dropped to around 45%. It is, therefore, very important to be able to detect the presence of anthrax early if its presence is suspected.[4]

In the United Kingdom (UK), anthrax is classified as a class three biological material, which means it can only be used and tested in highly regulated circumstances.[5] A substitute *Bacillus* species has been used because of its similarity in physical properties and cellular makeup: *Bacillus Subtilis var Niger*, also known as *Bacillus globigii* or BG for short.[6] This species is not dangerous to humans and can, thus, be used as a safe substitute. Multiple tests have been developed for the detection, specifically of BG spores, based both on immunoassay[7] and polymerase chain reaction (PCR)[8] methods.

Testing for the presence of *Bacillus athracis* can be challenging. It is very similar to another *Bacillus* species, that of *Bacillus cereus*,[9,10] which occupies the same environment as *B. athracis*.[11] With many shared characteristics and protein chains, it is difficult to differentiate between the two species. Most testing occurs in specialized laboratories equipped to deal with the pathogen, where nasal swabs or blood samples (if taken from humans) or environmental samples are taken and the bacteria are grown on agar plates, after which a myriad of tests are performed to confirm the presence of *B. athracis*.[12] Alternatively, there are commercial biosensors available that can give a result within 15 min from the sample collection, but they have a very high limit of detection and can give false negatives, which might, in turn, provide a false sense of security to the on-site responders.[13] Anthrax detection on-site is also difficult as the number of spores present can be quite small, especially in the collected air samples. Hence, there is a need for better and quicker on-site detection.[14]

Well-established methods for detection, including cell culturing, PCR, and immunoassays like enzyme-linked immunosorbent assay (ELISA), have been used for anthrax detection for decades. These methods are robust and reliable but often trade speed for low detection thresholds.[15]

Cell culturing relies on growing bacteria colonies on agar gel, which provides fertile conditions and can give a result for a concentration as low as 2.5 colony forming units

[a)]This paper is part of a special issue on Theory and Applications of Acoustofluidics.
[b)]ORCID: 0000-0001-6448-9448.
[c)]Electronic mail: P.Glynne-Jones@soton.ac.uk

 0001-4966/2021/149(6)/4228/11/$30.00

https://doi.org/10.1121/10.0005278

(CFU)/ml. The procedure is straightforward and takes a few days, but because of the similarity between various *Bacillus* species, extra tests need to be performed.[16]

Immunoassay methods are the cornerstone of anthrax testing and rely on specific antibodies to immobilize, concentrate, count, and visualize the pathogens. They are considerably faster than cell culturing (around a day) and can still provide low detection limits (10^0–10^4 CFU/ml), depending on the type of method used.[15] There are multiple methods for detecting *B*. anthracis spores based on the immunoassay principle,[12] and the only anthrax field testing kit on the market is immunoassay based and, while it can give results within 15 min, its detection limit is only 10^5–10^6 CFU/ml.[13] The biggest problem arises from the specificity of the antibodies used as, like with cell culturing, many species of the *Bacillus* family share similar properties, especially *B*. *cereus*.[17]

PCR relies on isolating, amplifying, and quantifying short deoxyribose nucleic acid (DNA) sequences. It has become a staple in detection methods due to its speed (3–24 h) and accuracy (10^0–10^6 CFU/ml, depending on the method).[15] In practice, contaminating DNA can create noise, and faster variants do not reliably tell if a cell is viable,[18] and detection limits below 100 CFU/ml are hard to achieve.[19,20] However, nucleic-based methods are becoming a new standard in anthrax detection.[21]

A. Concentration and delivery methods

Rapid anthrax detection at low concentrations is vital for rapid response. Commercial field kits have a high limit of detection and, therefore, require either a concentration phase or can only be applied in situations in which there is a high concentration of anthrax in the area.[13] Relying on diffusion alone takes prohibitively long (as will be demonstrated in Sec. V).

Newer biosensor methods attempt to combine speed and accuracy often through sample processing steps that capture and concentrate the pathogen before detection.[22] The methods of delivering the pathogen vary and usually double as the concentration step. The simplest method is to use gravity, but this scales very poorly and is static. An improvement would be to introduce flow and combine it with a method of directing and concentrating the pathogens. Several methods have been developed to improve this efficiency, including magnetophoresis, dielectrophoresis, and the focus of this paper—acoustophoresis.

Acoustic radiation forces have been used for decades as a method of manipulating particles.[23] It has the ability to move particles in bulk[24] but without damaging them and keeping their viability preserved.[25,26] In high flow scenarios, a device made by Carugo *et al*. managed to increase the concentration of bacterial cells 60-fold.[27] If latex particles are used in conjunction with *Escherichia coli*, up to 95% can be captured using the secondary acoustic radiation forces between the seed particle and bacteria to assist capture. With this method, even submicron particles down to 110 nm can be focused[28,29] and exhibit an increase in detection up to 128-fold.[30] Ultrasound (US) is incorporated in some *in situ* systems in which rapid detection is necessary: Ohlsson *et al*. demonstrated a device that uses ultrasound to separate, trap, and wash red blood cells and deliver them to a PCR chip for analysis. They managed to attain a limit of detection of 10^3 *Pseudomonas* bacterial CFU/ml in 2 h.[31] Real-time detection is a long sought-after goal for a lot of field tests, and Bavli *et al*. have managed to create a real-time monitoring device that uses ultrasonic standing waves (USWs) combined with latex-beads to achieve a limit of detection of 1.6×10^4 CFU/ml for *E*. *Coli* and 4×10^4 CFU/ml for *Salmonella enterica*, both in water.[29] This is a significant improvement over the tests that do not use ultrasound. BG spores often are used as a safe substitute for anthrax, and a few groups have worked with them to develop methods for anthrax detection. By using USW with an optical metal-clad leaky waveguide (MCLW) sensor, Zourob *et al*. achieved a detection limit of 10^3 CFU/ml, which is a 100-fold upgrade over the MCLW alone.[32] Martin *et al*. combined a quarter-wave (QW) device with an immunosensor surface, increased the capture efficiency of BG spores 70 times, and achieved a detection limit of 10^4 CFU/ml.[33]

The device developed in this paper is a proof-of-principle device for a portable system that can rapidly concentrate anthrax spores for subsequent rapid assays. The focus is on the development of the concentration and capture stage of the system whereby an acoustic resonance is used to push disperse spores in a fluidic sample toward a surface functionalized with antibodies to capture them. Spore staining is used to demonstrate the capture; however, development of a more robust and sensitive detection stage forms future work.

II. BACKGROUND

A. Acoustic radiation forces

In a standing wave field, a particle experiences radiation forces that are approximated by[34]

$$F_{\mathrm{PRF}} = -\frac{4\pi a^3}{3}\left(f_1 \frac{1}{2\rho_0 c_0^2}\nabla\langle p^2\rangle - f_2 \frac{3\rho_0}{4}\nabla\langle v^2\rangle\right), \quad (1)$$

where ρ_0 and c_0 are the density and speed of sound, respectively, of the surrounding fluid, and p and v describe the pressure and velocity fields, respectively, surrounding the particle, and a is the radius of the spherical particle. The two dimensionless correction factors, f_1 and f_2, are given as

$$f_1(\tilde{\kappa}) = 1 - \tilde{\kappa}, \quad \text{where} \quad \tilde{\kappa} = \frac{\kappa_p}{\kappa_0}, \quad (2a)$$

$$f_2(\tilde{\rho}) = \frac{2(\tilde{\rho} - 1)}{2\tilde{\rho} + 1}, \quad \text{where} \quad \tilde{\rho} = \frac{\rho_p}{\rho_0}. \quad (2b)$$

Here, $\tilde{\kappa}$ represents the compressibility ratio between the particle and fluid, and $\tilde{\rho}$ represents the density ratio between the particle and fluid. Typical particles (like BG spores) that are less compressible and denser than the medium are,

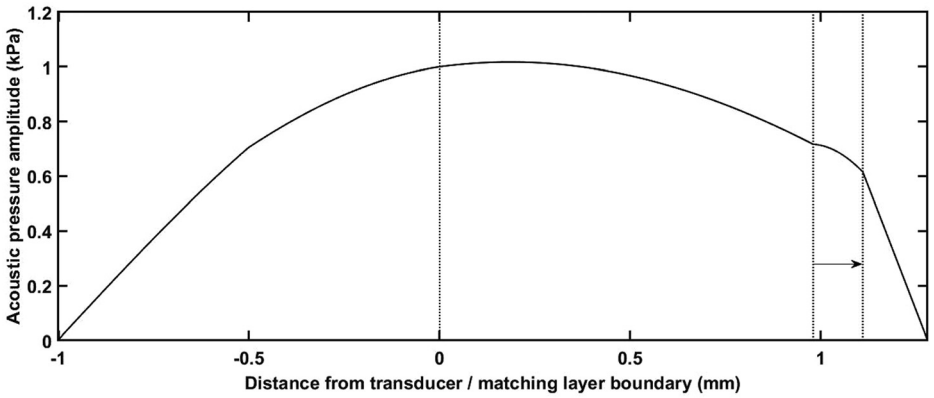

FIG. 1. The acoustic pressure amplitude, in kPa, is shown through all of the layers of the device. The entire device supports a half-wavelength structural mode with a pressure node at each boundary of the device. The four layers inside the device are, from left to right, transducer, carrier (matching), fluid, and reflector. The arrow highlights the consistently positive force toward the reflector layer surface.

therefore, attracted to the positions related to the pressure nodes and velocity antinodes [which are coincident in a one-dimensional (1D) standing wave field].

Because the acoustic radiation force is approximately proportional to the particle volume, the acoustic forces on the bacteria can be much smaller than those on other, larger cell types. In our device, we estimate the pressure amplitudes to be on the order of 500 kPa, which is sufficient to move the bacteria across the 130 μm channel height during a dwell time of order 3.5 s (see Sec. III B).

B. Layered acoustic resonators

The properties of the layers inside an acoustic resonator can be tuned in such a way that there are one or more pressure nodes inside the fluid channel. The nodes create planes toward which (for typical particles) the particles will move.[35] A special and prominent case in which there is one pressure node in the center of the channel is known as a half-wave device.[36] If, however, the particles are to be pushed toward a functionalized reflector layer, there are two options using bulk acoustic waves: QW devices and thin-reflector mode devices. The QW devices are carefully designed so that the pressure node lies exactly on the boundary between the fluid and reflector layer.[37] That way, all of the particles will tend to move toward that boundary. The problem with this type of device is that the heights of the different layers need to be extremely precise for it to work, and nonuniformities of the field across a device width will tend to cause regions in which particles do not reach the surface.[35] The thin-reflector mode device uses the first structural resonance of that device to create a standing wave pattern throughout all of the layers with the pressure node on the outer boundary of the reflector layer. In this configuration, the term "reflector" is a convention as the reflection actually occurs at the final device–air interface. This alternative operating mode makes the design far more robust as it can tolerate small changes of layer thicknesses easily.[38] It was, thus, considered the best choice for the device in this study.

III. ACOUSTIC AND MICROFLUIDIC DEVICE DESIGN

A. Layered resonator design

To set up an appropriate acoustic resonance, the device dimensions in the direction of the acoustic propagation were initially chosen using a 1D transfer impedance model developed by Hill *et al.*[39] Figure 1 shows the modelled distribution of the acoustic pressure through the device, whereas Fig. 2 shows the acoustic radiation force on a 1 μm particle at different positions in the channel. It can be seen that with this combination of layer thicknesses, the design creates a positive force toward the glass reflector capture surface from all positions within the fluid layer. The model also shows that the force is stronger near the glass surface and in contrast to a QW design,[35] creates a reliable positive force toward the antibody functionalized surface.

The device was designed such that the glass capture layer could be removed (rather than bonded to the other parts of the device) and is shown in Fig. 3. It consists of a lead zirconate titanate (PZT) transducer (1 mm thick;

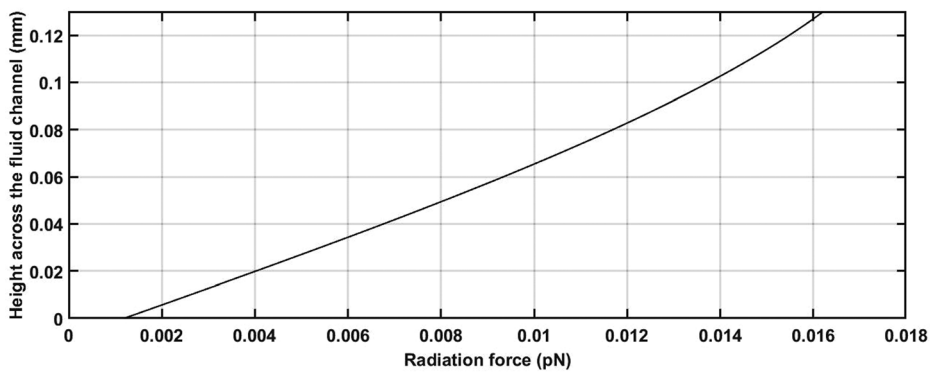

FIG. 2. The radiation force on a 1 μm particle as a function of the height across the fluid layer. The matching/fluid layer boundary is located at a height of 0 μm, whereas the fluid/reflector layer boundary is at 130 μm.

https://doi.org/10.1121/10.0005278

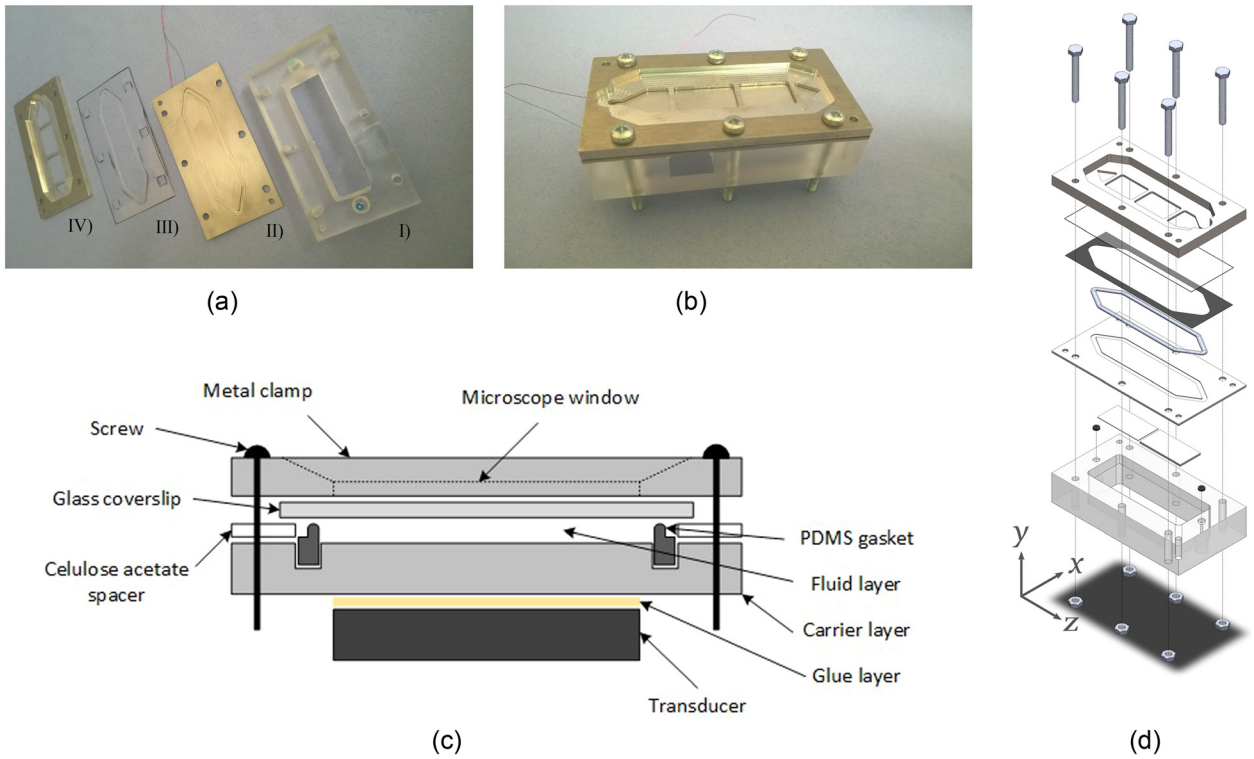

FIG. 3. (Color online) The images and schematics of the device design (a) disassembled, (b) assembled, (c) cross section schematic, and (d) exploded schematic. In the disassembled image, the labeled parts are (I) manifold, (II) metal carrier layer with transducer glued underneath, (III) cellulose acetate spacer, and (IV) metal clamp.

FerroPerm PZ26, Humlebaek, Demark) cut into a 24×12 mm rectangle, secured to a stainless steel carrier layer with epoxy (Epotek 301, Billerica, MA). The stainless steel sheet has a $\sim$100 μm recess milled inside it to hold the gasket. The gasket was cast out of polydimethylsiloxane (PDMS) and placed inside the groove to provide the side boundaries of the fluid layer, the bottom being the carrier layer and the top is the reflector layer. A spacer was cut from a 130 μm thick cellulose acetate sheet and placed concentrically with the gasket such that it controls the fluid channel height and ensures planarity and constant height. On top of the gasket and spacer lies a 170 μm glass coverslip thin-reflector layer. The chamber side of the reflector layer is functionalized with antibodies to capture specific pathogens (see Sec. IV). The layers are held in place with six bolts and sandwiched between a custom acrylic manifold on the bottom and a steel frame on top. The steel frame has a window so that the fluid channel can be observed with an optical microscope. The inlet and outlet tubings are connected to the manifold, which conveys the sample through two small holes in the carrier layer. The thicknesses and properties of all of the layers can be seen in Table I.

B. Device characterization

Because they have a volume similar to that of the target spores and are easy to visualize under a fluorescence microscope, 1 μm fluorescent beads (YG Fluoresbrite microspheres, Polysciences Inc., Bergstrasse, Germany) were initially used to assess the device properties. The device resonant frequency was established through electrical impedance measurements. Previous work has explored the connection between the electrically observed resonance and accompanying acoustic resonances of the coupled system.[35,38,39] Essentially, electrical resonances typically indicate an electromechanical resonance in the system, but modelling and observation are required to determine whether a particular electrical feature corresponds to the required acoustic mode. An impedance analyzer (Cypher Instruments C-60, London, UK) was used to measure the

TABLE I. Layer thickness and modelled material properties of the device. The thickness normalization was performed on the wavelength of 922 kHz, which is the mean resonant frequency of the device.

Layer	Thickness (μm)	Thickness/λ	Material	Density (kg/m^3)	Speed of sound (m/s^2)	Acoustic impedance (Mrayl)
Transducer	1000	0.182	PZ26 (Ferroperm)	7700	4530	34.9
Carrier	980	0.140	Stainless steel	7890	5790	45.7
Fluid	130	0.072 ($\ll\lambda$)	PBS	$\sim$1000	1480	1.5
Reflector	170	0.024 ($\ll\lambda$)	Glass	2500	5872	14.7

conductance of the device both when empty and when containing phosphate-buffered saline (PBS) as seen in Fig. 4. The resonance corresponding to the thin-reflector mode is seen as an unambiguous peak in the PBS-filled spectrum.

Resonant devices such as these are sensitive to the precise driving frequency relative to the natural resonance, and when the device was assembled before each experiment, small changes were observed, presumably as a result of small differences in the chamber height. The mean resonant frequency of the device was 922 ± 29 kHz. To allow for this and also accommodate small changes caused by the temperature and mechanical drift, the resonance was measured after assembling the device in each experiment and a frequency sweep (50 ms period) of ±10 kHz was used around the electrically measured resonant frequency. The sweep period (50 ms) was the minimum achievable with the signal generator (TG200; TTi, Huntingdon, UK). Previous work has shown that sweeps with periods of this order can be considered as comparable to a single force, which is the average of the force produced by each component frequency.[40]

To evaluate the effectiveness of acoustic forces to manipulate particles toward the glass surface, bead distributions before and after sonification were measured. A number of "*z*-stacks" were taken, meaning a sequence of images over a range of focal depths at a single lateral position within the channel. *Z*-stacks were taken at seven positions within the channel, corresponding to distances of 6, 12, 18, 24, 30, 36, and 42 mm from the outlet port along the device centerline on the axis of flow. Those highlighted in bold lie over the transducer. For each measurement, a fresh sample of randomly distributed beads was flowed into the device, the flow was stopped, and then the ultrasound was turned on for 10 s with a drive voltage of 30 Vpp applied to the transducer. The results are shown in Fig. 5, where it can be observed that, particularly over the transducer (positions 12, 18, and 24 mm), beads are moved toward the glass capture layer. The focal depth of the objective is around 10 μm, so these results do not demonstrate whether the beads are in contact with the glass but do provide evidence that above, the transducer beads are forced from all positions within the fluid depth toward the glass surface. In addition to the acoustic radiation force, there is a possibility of acoustic streaming at the 30 Vpp amplitude used. The concentration that was observed suggests that acoustic streaming (which would tend to disrupt the observed focusing) did not play a major role in this experiment. This was also backed up by observations by microscopy during the experiments, which did not show the rotational motion that streaming would produce.

In addition to the required forces in the height direction, lateral modes within the device[35] cause movement of suspended particles across its width. To assess this and also visualize the position in the device where the majority of beads first reach the capture surface, the montage seen in Fig. 6 was created. A plain glass slide (not functionalized) was used as it was found to capture a large proportion of beads that reached its surface. Beads (10^5 beads/ml) were pushed to the surface for 10 min of flow at 10 ml/h with ultrasonic focusing, then the ultrasound switched off and unbound beads were flushed out with de-ionized water. Images were taken across the device and assembled into the montage. The area with no transducer does not show a significant number of beads captured. Over the transducer, the effect of lateral forces can be seen in the visible lateral banding. The leading edge does not see significant beads attached, but after about 1 mm, a "touch-down" point is seen (the position varies across the width in a pattern that is consistent with a stronger acoustic field near the center of the device[35]). This point will relate to the distance that beads travel in the acoustic field before they reach the surface. Knowledge of the distribution of the particle capture is important as it will inform decisions over which parts of the surface to functionalize with antibodies for the most effective capture.

IV. METHODS

A. Spore preparation

The spore chosen as an analog for *B. anthracis* in these experiments was BG (obtained from Dstl, Porton Down, UK). The spores were initially washed using centrifugation at 3000 rpm for 3 min with the supernatant pipetted out and the spores resuspended with sterile de-ionized water. This process was repeated 4–6 times to reduce debris and spore fragments that might block the antibody surface, then the concentration was assessed with a haemocytometer.

To stain the spores, AlexaFluor 555 dye (ThermoFisher, Basingstoke, UK) was used. To a single

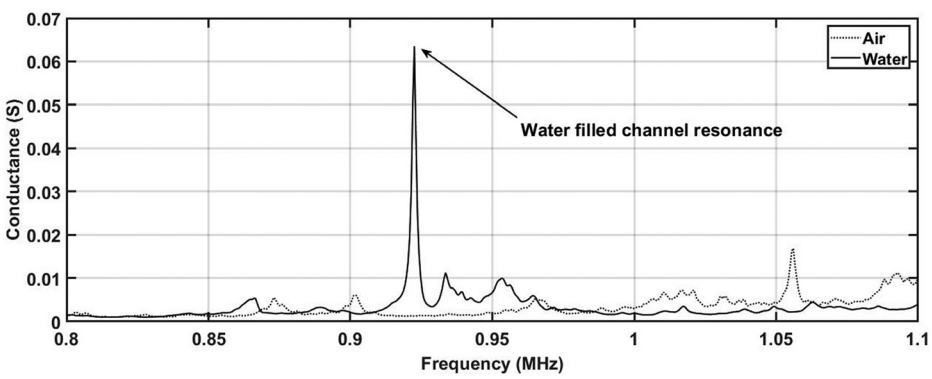

FIG. 4. The conductance plot of the device when it is filled with air or PBS. The clear peak around 0.93 MHz in the PBS-filled device is the thin-reflector mode resonance.

https://doi.org/10.1121/10.0005278

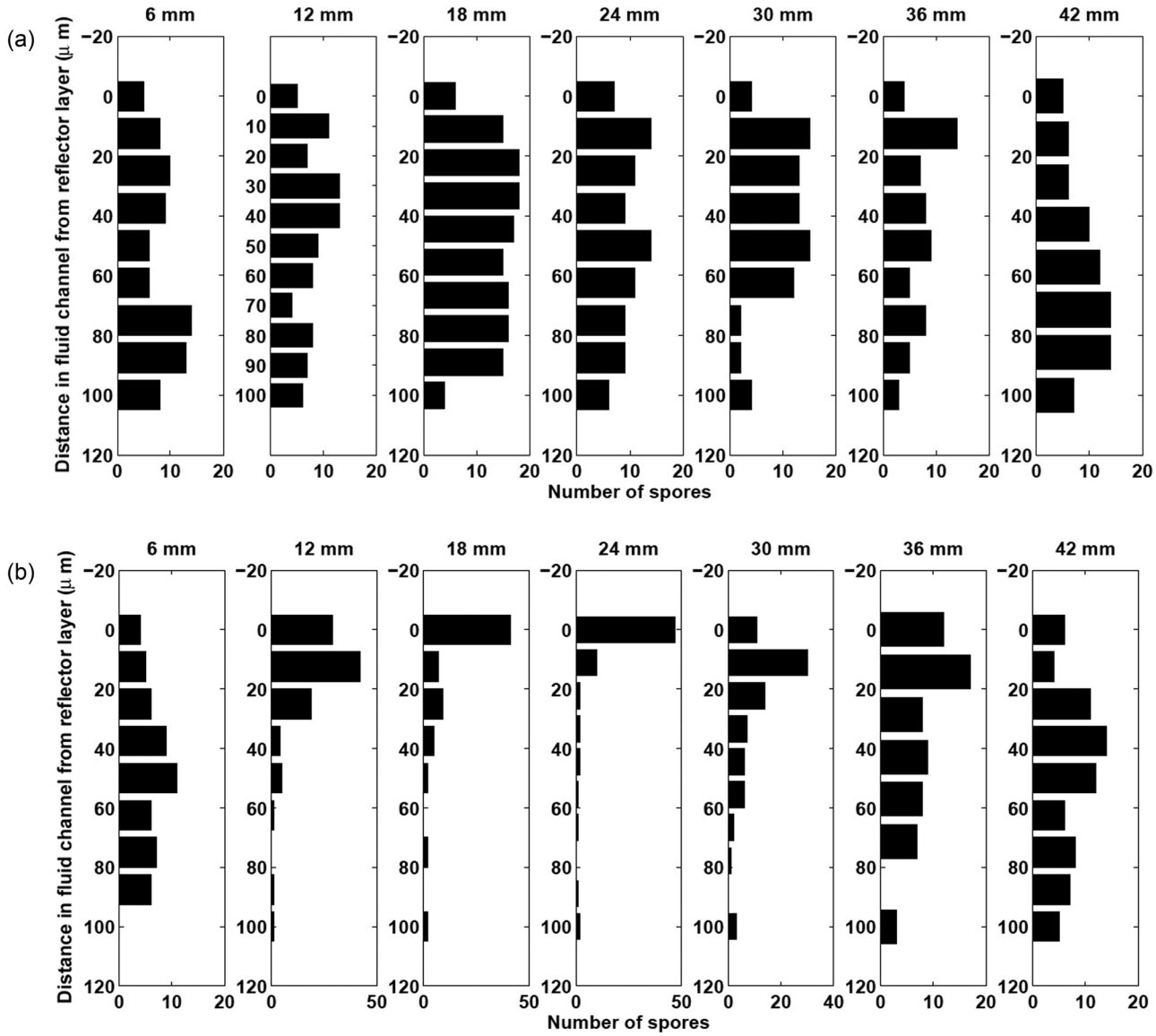

FIG. 5. The distribution of fluorescent beads through the height of the channel (a) before and (b) after 10 s of ultrasound exposure. The distance on top of each measurement refers to the distance along the centerline from the outlet toward the inlet.

100 μg vial of the dye, 10 μl of dimethyl sulfoxide (DMSO) was added. An aliquot of 500 μl of spore suspension at 10^9 CFU/ml was added to 500 μl of PBS, after which 10 μl of the dye/DMSO solution was added. The spores were incubated in a fridge at 4 °C, overnight. After incubation, they were again washed in de-ionized water with centrifugation and stored in a fridge and in the dark to prevent germination and photo-bleaching, respectively. When used in an

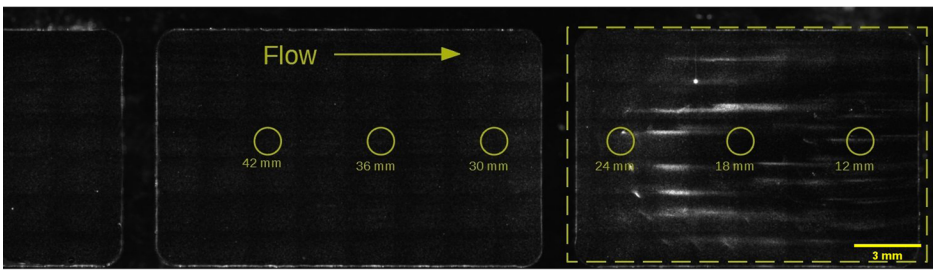

FIG. 6. (Color online) The montage image shows the distribution of beads captured on an untreated glass surface. The circles indicate the sampling positions used in Fig. 5. The dotted outline shows the position of the transducer relative to the channel. The vertical bars are the outlines of the window in the metal clamp. The b eads are seen to begin to adhere at around 1.5 mm from the transducer edge and significant lateral banding can be seen.

experiment, the spores were resuspended in PBS to the required concentration.

B. Antibody functionalization of slides

The slides (Nexterion, Slide E, Schott, Germany) were functionalized with BG specific antibodies (Rabbit anti-B globigii IgG antibody, Tetracore, Rockville, MD). They were pre-coated with a polyethylene glycol (PEG) "forest," which can be linked to antibodies but also reduces nonspecific binding in areas that are not functionalized.

The antibodies were diluted in PBS to a concentration of 0.25 mg/ml. An aliquot of 0.25 ml was pipetted onto the slide, and a glass coverslip was positioned on top of the aliquot to ensure coverage of the required region and to prevent evaporation. The coverslip was held away from the surface by a spacer that was ∼80 μm thick, effectively forming a small temporary chamber. Figure 7 shows the active area of the slide and relative position of the functionalization. The slides were then suspended in a sealed humidity chamber that had a 25 mm deep layer of saturated sodium chloride solution at the bottom. The slides were left in the chamber overnight at room temperature. The next day the slides were removed from the chamber and placed in a slide holder filled with a 1% bovine serum albumin (BSA) solution for 1 h. This was done to further reduce nonspecific binding. Once removed, the slides were gently rinsed with PBS and dried using a stream of dried air from a compressor.

A control experiment required the use of nonspecific antibodies. The antibody used was anti-human CD203c basophil[41]-specific antibody (Miltenyi Biotec, Surrey, UK). The binding procedure was the same as that described above.

C. Spore capture protocol

Capture experiments were performed with ultrasound and antibodies in addition to controls with (a) no ultrasound and (b) nonspecific antibodies. For each condition, three repeats were performed. Where used, ultrasound was activated with a frequency sweep (50 ms period) of ±10 kHz around the electrically measured resonant frequency and driving voltage of 10 Vpp (see Sec. III B). Spores were pumped through the device using a syringe pump (Harvard Apparatus Pump 11 Elite, Cambridge, UK) at a concentration of 102 spores/ml at a rate of 30 ml/h. Inside the syringe, a 3 mm stirring magnet was placed and rotated to ensure that the spores did not settle during the experiment. After 10 min of spore capture under flow (a total sample volume of 6 ml), the ultrasound was switched off, and PBS was flowed through the fluid channel at the same rate for 2 min to remove any spores that were not captured by the antibody layer. Finally, air was passed through the channel to remove any PBS, further reducing the chance of accidental spore capture outside of the assay period. The device was disassembled, and the slide was rinsed again in PBS and dried with a stream of dried air from a compressor. The reusable components of the device were washed with denoised water and dried using microscope tissues and air prior to the next experiment. The slides were stored in a dry and dark container at room temperature. Figure 8 shows the system configuration of the hardware used.

Once removed from the device, the slides were imaged with an inverted epi-fluorescence microscope (Olympus IX71, Tokyo, Japan). An automated XY stage (Thorlabs MLS203, Basingstoke, UK) acquired a 10 × 10 mosaic of fluorescent (FITC filter cube, Tokyo, Japan) images in the region marked in Fig. 7. This covered an area of 8.8 mm × 6.7 mm. A Hammamatsu ORCA-ER camera and 10× objective (Olympus UPLFLN 10×, Tokyo, Japan) was used. Micro-manager, an open source microscopy software[42] was used to control the XY stage. The brightness and contrast of the images were adjusted to aid visualization, and the number of spores in each frame was counted manually.

V. RESULTS

To highlight the advantage of using ultrasound and provide a baseline, the rate of sedimentation of the spores by themselves was assessed. A test was performed with the spores on a haemocytometer (Hausser Scientific Neubauer Improved HL, Horsham, PA) whose chamber has a height of 100 μm, which is roughly the same as that of the ultrasonic device (130 μm). The 134 spores, which were present in the chamber, would initially be equally distributed across the volume. After 25 min, all spores have sedimented as shown in Fig. 9; a linear fit shows that spores sedimented at a velocity of 3.6 μm/min.

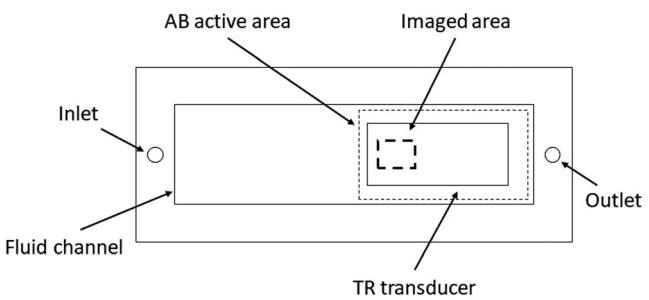

FIG. 7. The relative positions of the antibody (AB) functionalized area to the transducer and imaging regions in the device.

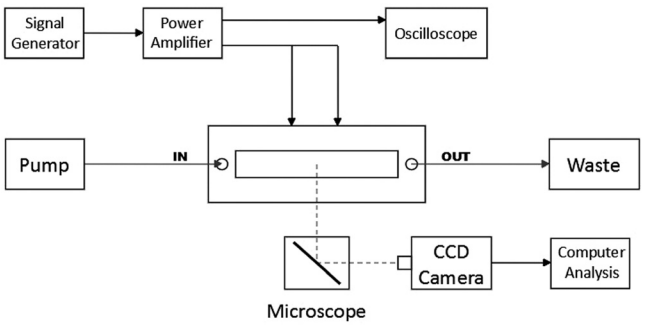

FIG. 8. The schematic of the system configuration.

https://doi.org/10.1121/10.0005278

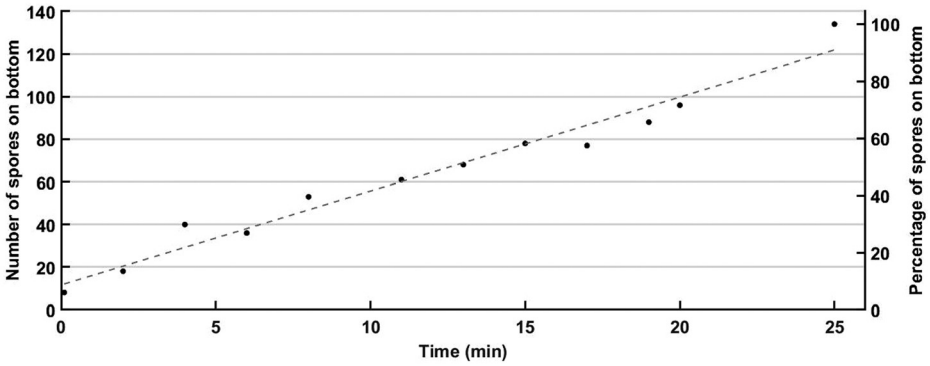

FIG. 9. The graph depicting the sedimentation of spores on a haemocytometer with a liquid layer with a height of 100 μm. The data are presented as both the raw number of spores and a percentage. A trendline was fitted to the data.

The results are reported for a suspension of 10^2 spores/ml. Two controls are included: no ultrasound but with the correct antibody and ultrasound turned on but with the "wrong" (i.e., nonspecific) antibody. Figure 10 shows the mean values of the spore counts performed for all of the test conditions outlined in this paragraph. The values of the spore count for each experiment, as listed in Table II, are overlaid as individual points over the corresponding bars. On average, without ultrasound, 70 spores or 14% of all spores were captured (likely due to diffusion). When the wrong (nonspecific) antibody was used, 140 spores or 28% of all spores, on average, were captured. When both ultrasound and the correct antibodies were present, the mean spore capture was 299 spores or 60% of all spores that passed through the device.

VI. DISCUSSION

The terminal velocity of a spore as it sediments is determined by[43]

$$u_{\max} = \frac{d^2(\rho_s - \rho)g}{18\mu}, \tag{3}$$

where d is the diameter of the spore, ρ_s is the density of the spore, ρ is the density of the surrounding medium, g is the acceleration due to gravity, and μ is the dynamic viscosity of the surrounding fluid. The BG spore diameter (0.6 μm) and density (1200 kg/m^3) were found using information from two papers by Carrera *et al.*[2,44] BG spores are elliptical in shape with an almost 2:1 ratio,[2] but they were approximated to be a spore of the same volume for the terminal velocity equation because both the size and velocity are very small.[43] The value used for the viscosity of water at 20 °C was 1.002 mPa s,[45] and the density value was taken as 1000 kg/m^3. The terminal velocity was found to be 2.5 μm/min, which is very similar to the experimental value of 3.6 μm/min. The sedimentation (Fig. 9) was performed as a baseline and a worst-case scenario—i.e., if no other force is applied, it indicates how long it will take to capture the spores by just letting them sediment.

Approximately 500 spores passed through the device during the lowest concentration experiments. Without the aid of ultrasound, only 70 spores were captured, on average, in the imaged area. This amounts to 14% of the total spore number that passed through the fluid channel. With a 30 ml/h flow, the velocity inside the fluid chamber is 6.94 mm/s (calculated by dividing the flow rate by the cross sectional area of the fluid channel[43]), meaning that a spore spends a total of 8.96 s inside the fluid chamber.

Figure 11 shows how a spore would travel through a 100 μm fluid channel with a parabolic velocity profile and constant downward velocity. The value for the downward velocity was found experimentally from the sedimentation test, whereas the average velocity in the channel from which the velocity profile was found was calculated in the paragraph above. The velocity profile is given by[43]

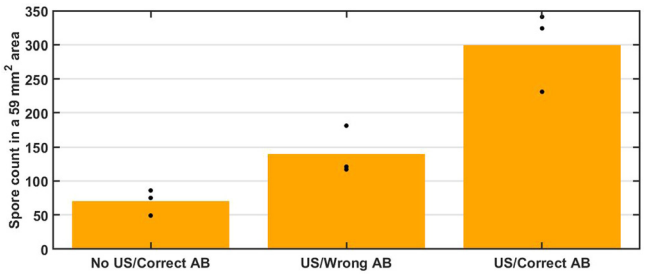

FIG. 10. (Color online) The mean values (bars) and values for each repeat (dots) of the spore capture experiments for the three different conditions: no US with the correct antibody (AB), US but with the wrong AB, and US with the correct AB.

TABLE II. Spore counts for all of the experimental repeats under all conditions.

Concentration (CFU/ml)	US	Antibody	Repeat number	Total count
			1	75 (15%)
10^2	No	BG	2	49 (9.8%)
			3	86 (17.2%)
			1	121 (24.2%)
10^2	No	CD203c	2	181 (36.2%)
			3	117 (23.4%)
			1	341 (68.2%)
10^2	Yes	BG	2	324 (64.8%)
			3	231 (46.2%)

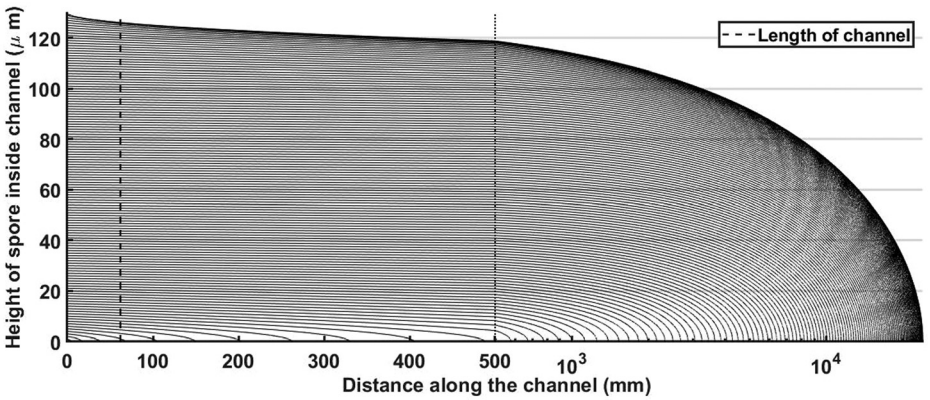

FIG. 11. A simulation of a path that a spore-sized spherical object would take inside the channel with a parabolic velocity profile and constant downward velocity. The x axis is linear to the left of the dotted line (···) located at the 500 mm mark and it is logarithmic to the right. The dashed line at 62 mm (—) represents the length of the physical fluid channel. Any sphere that touches down (reaches a height of 0 mm) before it can be assumed to be captured. Only 3% of the spheres were captured this way.

$$u(r) = u_{\max}\left[1 - \frac{r^2}{R^2}\right], \tag{4}$$

where r is the distance from the centerline, R is half the height of the channel, and $u_{\max}$ is the maximum velocity in the channel, which is also expressed as

$$u_{\max} = 2u_{\text{average}}. \tag{5}$$

A sphere with the diameter of the spore was simulated for every possible height in the channel in 1 μm intervals. Figure 11 shows the trajectories that each of the spheres take, whereas the dashed line marks the end of the physical channel in the device. The number of spheres that touch the surface only account for 3% of the total spheres simulated. The difference can be explained by the fact that the simulation assumes perfect laminar conditions. Because the chamber inlet is a lot smaller (a tube of 1 mm in diameter), the velocity at the inlet would be higher than in the chamber for a given volume flow rate. This means that at the inlet, possible disturbances resulting from the device geometry may occur, which might change the equal distribution of the spores assumed by the model. Figure 11 uses a nonuniform x axis distribution: to the left of the dotted line (···), the x axis is linear (between 0 and 500 mm), and to the right of the line, it is logarithmic, base 10.

Ultrasound enables more spores to reach the antibody coating, but if the coating is specific to a different receptor (as is the case with CD203c), the spore will not attach and will roll away. It is quite possible, however, that the capture rate for these experimental conditions could be even lower as the technique used to coat the slides (described in Sec. IV B) could be optimized to further reduce nonspecific binding.

When the antibody is specific to the spores, the capture rate increases from 28% to 60% of all of the spores that pass through the device.

The imaging area is 59 mm^2, whereas the total active area is 288 mm^2. The total imaged area is, therefore, only 20% of the active area. However, as seen in Fig. 6, a lot of the particles touch down very early in the active area (the crescent shape in Fig. 6). Furthermore, the width of the imaged area makes 55% of the width of the active area and is located centrally, where the flow is faster and, hence, more spores pass through. With such advantageous positioning of the imaged area, it is reasonable to expect a higher detection proportion compared to the area proportion. On average, there were three spores per image; however, they were not equally distributed throughout the imaged area.

In their article, Martin *et al.*[33] describe a device which uses a QW USW to capture BG spores at a concentration of 2×10^4 spores/ml. They started with a batch mode in which a spore suspension was brought into the device and insonified. A mean time of 35 s was enough to capture 95% of all available spores. In a second experiment, Martin *et al.* demonstrated that a similar capture rate could be achieved while flowing the sample at 6 ml/h.

They predicted that with this technology—the combination of an immunoassay with an USW—capture and detection were possible at concentrations as low as 200 CFU/ml with an assay time of 25 min while still maintaining the capture rate close to 100%.[33]

Our device, operating at a 200-fold lower concentration than described by Martin *et al.*,[33] demonstrates that their prediction was accurate, capturing 60% of all spores at a concentration of 100 CFU/ml. If the imaging window size was increased (or another detection method used that did not rely on imaging only a proportion of the ultrasonically active areas), the capture rate might be increased. Low concentration spore detection is not only possible but viable with a method that combines immunoassays with USWs.

Furthermore, by employing the alternative thin-reflector mode, we have produced a device that can be readily manufactured and would be more robust that a QW device. It is less sensitive to minor geometry and height changes as might be found during manufacture, and it can be tuned with a broader range of layer thicknesses.[35]

This device was created as proof-of-principle for low concentration spore capture and as such, the detection technique was primitive and needs further work to realize a complete system. It is capable of detecting concentrations of 100 spores/ml with an assay time of 10 min, but it cannot count close to 100% of their number due to the limited imaging area. Nonetheless, even at this level of performance, it is comparable with other devices and biosensors that have some of the lowest detection thresholds. To make the device usable in the field, it would need to be combined with a suitable capturing method that would

allow for quick or real-time detection. There are already examples of using acoustic detection combined with PCR,[31,46] and the use of mass spectrometry or Raman spectrometry looks very promising as a detection method.[19] Coupled with an acoustic concentration and immuno-capture, it could be made into a very quick, robust, low-cost, and easy to use device that could be deployed on the field for both water and air safety testing.

VII. CONCLUSION

Driven with a frequency sweep of 20 kHz centered around a mean resonance of 922 kHz, the device presented in this paper was able to capture and detect spores at a concentration of 100 spores/ml. Using the thin-reflector mode created a system that was not sensitive to small changes in the layer thickness from manufacturing and assembly variations. In combination with an antibody coating on the reflector layer, 60% of the 500 spores that typically flowed through the device in a 10 min assay were captured. This number could be improved with a wider imaging area and automated imaging technique. This device is a proof of concept that spores can, indeed, be concentrated and detected at such low concentrations by using an acoustic immunoassay system. By pairing it with a better detection method (e.g., PCR or Raman spectroscopy), a field-worthy device could be created.

ACKNOWLEDGMENTS

Support under the Engineering and Physical Sciences Research Council (UK; EPSRC) Fellowship No. EP/L025035/1 is gratefully acknowledged. The authors would like to thank Martin McDonnell and DSTL at Porton Down for providing the BG spores and expertise in slide functionalization. All relevant data have been included in this paper.

[1]S. Shafazand, R. Doyle, S. Ruoss, A. Weinacker, and T. A. Raffin, "Inhalational anthrax: Epidemiology, diagnosis, and management," Chest **116**, 1369–1376 (1999).
[2]M. Carrera, R. O. Zandomeni, J. Fitzgibbon, and J.-L. Sagripanti, "Difference between the spore sizes of *Bacillus anthracis* and other *Bacillus* species," J. Appl. Microbiol. **102**, 303–312 (2007).
[3]W. S. Albrink, S. M. Brooks, R. E. Biron, and M. Kopel, "Human inhalation anthrax: A report of three fatal cases," Am. J. Pathol. **36**, 451–471 (1960).
[4]J. C. Holty, D. M. Bravata, H. Liu, R. A. Olshen, K. M. McDonald, and D. K. Owens, "Systematic review: A century of inhalational anthrax cases from 1900 to 2005," Ann. Internal Med. **144**, 270–280 (2006).
[5]Health and Safety Executive, "The approved list of biological agents," available at https://www.hse.gov.uk/pubns/misc208.pdf (Last viewed 28 March 2021).
[6]K. D. Chichester, D. B. Silcott, and C. L. Colyer, "Analysis of *Bacillus globigii* spores by CE," Electrophoresis **29**, 641–651 (2008).
[7]D. N. Stratis-Cullum, G. D. Griffin, J. Mobley, A. A. Vass, and T. Vo-Dinh, "A miniature biochip system for detection of aerosolized *Bacillus globigii* spores," Anal. Chem **75**, 275–280 (2003).
[8]P. Belgrader, D. Hansford, G. T. A. Kovacs, K. Venkateswaran, R. Mariella, F. Milanovich, S. Nasarabadi, M. Okozumi, F. Pourahmadi, and M. A. Northrup, "A minisonicator to rapidly disrupt bacterial spores for DNA analysis," Anal. Chem. **71**, 4232–4236 (1999).
[9]S. R. Klee, H. Nattremann, S. Becker, M. Urban-Schreifer, T. Franz, D. Jacob, and B. Appel, "Evaluation of different methods to discriminate *Bacillus anthracis* from other bacteria of the *Bacillus cereus* group," J. Appl. Microbiol. **100**, 673–681 (2006).
[10]V. I. Klichko, J. Miller, A. Wu, S. G. Popov, and K. Alibek, "Anaerobic induction of *Bacillus anthracis* hemolytic activity," Biochem. Biophys. Res. Commun. **303**, 855–862 (2003).
[11]X. Hu, I. Swiecicka, S. Timmery, and J. Mahillion, "Sympatric soil communities of Bacillus cerus sensu lato: Population, structure and potential plasmid dynamics of pXO1- and pXO2-like elements," FEMS Microbiol. Ecol. **70**, 344–355 (2009).
[12]L. M. Irenge and J.-L. Gala, "Rapid detection methods for *Bacillus anthracis* in environmental samples: A review," Appl. Microbiol. Biotechnol. **93**, 1411–1422 (2012).
[13]D. King, V. Luna, A. Cannons, J. Cattani, and P. Amuso, "Performance assessment of three commercial assays for direct detection of *Bacillus anthracis* spores," J. Clinical Microbiol. **41**, 3454–3455 (2003).
[14]C. F. Froncyek and J.-Y. Yoon, "Biosensors for monitoring airborne pathogens," J. Lab. Autom. **20**, 390–410 (2015).
[15]O. Lazcka, F. J. Del Campo, and F. X. Muñoz, "Pathogen detection: A perspective of traditional methods and biosensors," Biosens. Bioelectron. **22**, 1205–1217 (2007).
[16]R. W. Titball, P. C. Turnbull, and R. A. Hutson, "The monitoring and detection of *Bacillus anthracis* in the environment," in *Society for Applied Bacteriology Symposium Series* (1991), Vol. 20, pp. 9s–18s.
[17]D. D. Williams and C. L. Turnbough, "Surface layer protein EA1 is not a component of *Bacillus anthracis* spores but is a persistent contaminant in spore preparations," J. Bacteriol. **186**, 566–569 (2004).
[18]L. Garibyan and N. Avashia, "Polymerase chain reaction," J. Invest. Dermatol. **133**, 1–4 (2013).
[19]H. Wang, Y. Zhou, X. Jiang, B. Sun, Y. Zhu, H. Wang, Y. Su, and Y. He, "Simultaneous capture, detection, and inactivation of bacteria as enabled by a surface-enhanced Raman scattering multifunctional chip," Angew. Chem. Int. Ed. **54**, 5132–5136 (2015).
[20]A. Neimz, T. M. Ferguson, and D. S. Boyle, "Point-of-care nucleic acid testing for infectious diseases," Trends Biotechnol. **29**, 240–250 (2011).
[21]C. Ryu, K. Lee, C. Yoo, W. K. Seong, and H.-B. Oh, "Sensitive and rapid quantitative detection of anthrax spores isolated from soil samples by real-time PCR," Microbiol. Immunol. **47**, 693–699 (2003).
[22]A. E. Yousef, "Detection of bacterial pathogens in different matrices: Current practices and challenges," in *Principles of Bacteria Detection*, edited by M. Zourob, S. Elwary, and A. Turner (Springer, New York, 2008), pp. 31–48.
[23]Z. Mandralis, D. L. Feke, W. Bolek, W. Burger, and E. Benes, "Enhanced synchronized ultrasonic and flow-field fractionation of suspensions," Ultrasonics **32**, 113–122 (1994).
[24]A. Lenshof, C. Magnusson, and T. Laurell, "Acoustofluidics 8: Applications of acoustophoresis in continuous flow microsystems," Lab Chip **12**, 1210–1223 (2012).
[25]M. Hill and N. R. Harris, "Ultrasonic microsystems for bacterial cell manipulation," in *Principles of Bacteria Detection*, edited by M. Zourob, S. Elwary, and A. Turner (Springer, New York, 2008), pp. 909–928.
[26]H. Bohm, P. Anthony, M. R. Davey, L. G. Briarty, J. B. Power, K. C. Lowe, E. Benes, and M. Groschl, "Viability of plant cell suspensions exposed to homogenous ultrasonic fields of different energy density and wave type," Ultrasonics **38**, 629–632 (2000).
[27]D. Carugo, T. Octon, W. Messaoudi, A. L. Fisher, M. Carboni, N. R. Harris, M. Hill, and P. Glynne-Jones, "A thin-reflector microfluidic resonator for continuous-flow concentration of microorganisms: A new approach to water quality analysis using acoustofluidics," Lab Chip **14**, 3830–3842 (2014).
[28]B. Hammarström, T. Laurell, and J. Nilsson, "Seed particle-enabled acoustic trapping of bacteria and nanoparticles in continuous flow systems," Lab Chip **12**, 4296–4304 (2012).
[29]D. Bavli, N. Emanuel, and Y. Barenholz, "Real-time monitoring of *E. coli* O157 and *Salmonella enterica serovar Typhimurium* in water using ultrasound and latex-based immunoassay," Anal. Methods **6**, 395–403 (2014).
[30]M. A. Sobanski, R. Vince, G. A. Biagini, C. Cousins, M. Guiver, S. J. Gray, E. B. Kaczmarski, and W. T. Coakley, "Ultrasound enhanced detection of individual meningococcal serogroups by latex immunoassay," J. Clin. Pathol. **55**, 37–40 (2002).
[31]P. Ohlsson, M. Evander, K. Petersson, L. Mellhammar, A. Lehmusvori, U. Karhunen, M. Soikkeli, T. Seppä, E. Tuunainen, A. Spangar, P. von Lode, K. Rantakokko-Jalava, G. Otto, S. Scheding, T. Soukka, S. Wittfooth, and T. Laurell, "Integrated acoustic separation, enrichment,

and microchip polymerase chain reaction detection of bacteria from blood for rapid sepsis diagnostics," Anal. Chem. **88**, 9403–9411 (2016).
[32]M. Zourob, J. J. Hawkes, W. T. Coakley, B. J. Treves Brown, P. R. Fielden, M. B. McDonnell, and N. J. Goddard, "Optical leaky waveguide sensor for detection of bacteria with ultrasound attractor force," Anal. Chem. **77**, 6163–6168 (2005).
[33]S. P. Martin, R. J. Townsed, L. A. Kuznetova, K. A. J. Borthwick, M. Hill, and M. B. McDonnel, "Spore and micro-particle capture on an immunosensor surface in an ultrasound standing wave system," Biosens. Bioelectron. **21**, 758–767 (2005).
[34]H. Bruus, "Acoustofluidics 7: The acoustic radiation force on small particles," Lab Chip **12**, 1014–1021 (2012).
[35]P. Glynne-Jones, R. J. Boltryk, and M. Hill, "Acoustofluidics 9: Modelling and applications of planar resonant devices for acoustic particle manipulation," Lab Chip **12**, 1417–1426 (2012).
[36]A. Lenshof, M. Evander, T. Laurell, and J. Nilsson, "Acoustofluidics 5: Building microfluidic acoustic resonators," Lab Chip **12**, 684–695 (2012).
[37]J. J. Hawkes, M. J. Long, W. T. Coakley, and M. B. McDonnell, "Ultrasonic deposition of cells on a surface," Biosens. Bioelectron. **19**, 1021–1028 (2004).
[38]P. Glynne-Jones, R. J. Boltryk, M. Hill, R. Harris, and P. Paclet, "Robust acoustic particle manipulation: A thin-reflector design for moving particles to a surface," J. Acoust. Soc. Am. **126**, EL75–EL79 (2009).
[39]M. Hill, Y. Shen, and J. J. Hawkes, "Modelling of layered resonators for ultrasonic separation," Ultrasonics **40**, 385–392 (2002).
[40]P. Glynne-Jones, R. J. Boltryk, N. R. Harris, A. W. J. Cranny, and M. Hill, "Mode-switching: A new technique for electronically varying the agglomeration position in an acoustic particle manipulator," Ultrasonics **50**, 68–75 (2010).
[41]A type of white blood cell roughly 15 times bigger than a BG spore.
[42]A. D. Edelstein, M. A. Tsuchida, N. Amodaj, H. Pinkard, R. D. Vale, and N. Stuurman, "Advanced methods of microscope control using μManager software," J. Biol. Methods **1**, e10–e11 (2014).
[43]B. Massey, "*Mechanics of Fluids*," (Special Indian Edition), 8th ed. (Taylor and Francis, London, UK, 2010), Chap. 6, pp. 191–195.
[44]M. Carrera, R. O. Zandomeni, and J.-L. Sagripanti, "Wet and dry density of *Bacillus anthracis* and other *Bacillus* species," J. Appl. Microbiol. **105**, 68–77 (2008).
[45]"Water—Dynamic and kinematic viscosity," available at https://www.engineeringtoolbox.com/water-dynamic-kinematic-viscosity-d_596.html (Last viewed 27 March 2021).
[46]S. J. Gray, M. A. Sobanski, E. B. Kaczmarski, M. Guiver, W. J. Marsh, R. Borrow, R. A. Barnes, and W. T. Coakley, "Ultrasound-enhanced latex immunoagglutination and PCR as complementary methods for non-culture-based confirmation of meningococcal disease," J. Clin. Microbiol. **37**, 1797–1801 (1999).